Catalysis Today 175 (2011) 264–270

Contents lists available at ScienceDirect

Catalysis Today

journal homepage: www.elsevier.com/locate/cattod

TiO_2 promoted Ir/Al_2O_3 catalysts for direct decomposition of N_2O

Shuang Liu[a,b], Yu Cong[a], Yanqiang Huang[a], Xiangyun Zhao[a,b], Tao Zhang[a,*]

[a] State Key Laboratory of Catalysis, Dalian Institute of Chemical Physics, CAS, Dalian 116023, China
[b] Graduate School of the Chinese Academy of Sciences, Beijing 100049, China

ARTICLE INFO

Article history:
Received 31 October 2010
Received in revised form 28 January 2011
Accepted 26 February 2011
Available online 2 April 2011

Keywords:
Nitrous oxide
Catalytic decomposition
Iridium
TiO_2
Al_2O_3

ABSTRACT

TiO_2 promoted Ir/Al_2O_3 catalysts (Ir/TiO_2–Al_2O_3) were successfully used in direct decomposition of N_2O with high catalytic activities and good thermal stabilities. Application of different characterization techniques revealed that the activity enhancement was closely correlated with the properties of the support material. Iridium was highly dispersed over the binary system of TiO_2–Al_2O_3, due to the nanoscale rough surface and strong interaction between iridium and the support induced by TiO_2 addition. Enhanced capability of reversible oxygen adsorption was detected on the TiO_2 promoted sample, which also promoted the catalyst for N_2O decomposition.

1. Introduction

Nitrous oxide (N_2O) is a major greenhouse gas and a main substance damaging the ozone layer [1,2]. The largest single source of N_2O, with a total emission amount of 125 Mton CO_2-equiv. per year [3], is the nitric acid plants, where N_2O is formed as a by-product in the catalytic oxidation of ammonia over Pt–Rh alloy gauzes [4]. Direct decomposition of N_2O below the noble metal gauzes in the ammonia burner is regarded as a cost-effective abatement measure for existing plants. For such a process, extremely good thermal stability is required for the catalysts to withstand high temperatures of more than 800 °C [3].

On the other hand, nitrous oxide is also a promising green propellant for small satellite propulsion [5–8]. N_2O has a number of advantages, such as facilitating multiple propulsion modes, self-pressurizing, system simplicity as well as low-cost, associating with its non-toxicity and good compatibility with common construction materials. Detectable decomposition of N_2O can only take place at temperatures above 600 °C due to its high activation energy of ca. 250 kJ/mol, and it releases enormous heat leading to a maximum adiabatic temperature as high as 1600 °C. Upon the application of N_2O for advanced propulsion systems, catalytic decomposition is also an efficient choice to lower the decomposition temperature and accelerate the reaction rate. Therefore, to develop appropriate catalyst materials, which possess high catalytic activities at low temperatures and thermal stabilities at high temperatures, is of great importance.

Numerous catalysts have been developed for the direct decomposition of N_2O, such as pure and mixed oxides [9–11], transition metal-exchanged zeolites [12–14] and supported metal catalysts [15–20]. Among them, noble metal catalysts are known to have quite high activity, and Ir/Al_2O_3 was reported to be a promising representative [19,20]. However, the catalyst exhibited relatively lower initial activity at low temperatures in high-concentration (30–100%, v/v) N_2O decomposition for propulsion applications and was deactivated gradually at high temperatures due to the sintering of iridium, which greatly constrains its practical application. One effective strategy is to find a suitable support capable of stabilizing Ir particles and efficiently facilitating the decomposition of N_2O.

Addition of promoters to alumina has been extensively used to prevent the catalyst sintering and stabilize the noble metals [21–31]. For example, Barrera et al. have reported that the physicochemical properties, such as reducibility, oxidation of Pd and NO dissociative adsorption of Pd/Al–La catalysts, were all modified by La_2O_3 inclusion, and high N_2 selectivity at low temperatures (<250 °C) in the NO reduction with H_2 was obtained and attributed to the new adsorption sites created through the formation of a surface PdO_x phase interacting with La_2O_3 [21–23]. Kappenstein et al. have found that the introduction of silicon atoms stabilized the alumina defect structure, which made possible better thermal stabilization of the transition alumina and smaller crystallite size of the supported platinum particles, resulting in a good activity in catalytically decomposing aqueous HAN and HNF solutions

* Corresponding author. Tel.: +86 411 8437 9015; fax: +86 411 8468 5940.
E-mail address: taozhang@dicp.ac.cn (T. Zhang).

0920-5861/$ – see front matter © 2011 Elsevier B.V. All rights reserved.
doi:10.1016/j.cattod.2011.02.053

[24–26]. Ceria, zirconia and alkaline earth metal are also the most frequently cited additives to adjust the interaction between active metal and alumina support and to stabilize the noble metal particles [17,27–30,32].

But relatively little is known about TiO_2 modified alumina system. Yan et al. have developed an ultrastable Au nanocatalyst by the deposition of Au nanoparticles on the nanocrystalline TiO_2 surface-modified with an amorphous aluminum-oxide layer [33]. Lin et al. have reported that addition of TiO_2 into alumina enhanced the reduction as well as the oxygen mobility of palladium oxide and thus generated catalyst with much higher activity for the total oxidation of methane [34]. The Al_2O_3–TiO_2 system has also exhibited high activity and selectivity in hydrotreatment and NO abatement in virtue of its improvement in metal dispersion and sulfur-resistance [35–37]. However, probably due to the small specific surface area and low thermal stability of TiO_2, the TiO_2–Al_2O_3 system were commonly used at temperatures below 700 °C. Few studies were carried out by using TiO_2 to improve the thermal stability of alumina supported catalyst at high temperatures above 900 °C, and no catalytic data for N_2O decomposition over this system has been reported until now.

In the present work, we prepared a series of TiO_2 promoted Ir/Al_2O_3 catalysts, with the aim of developing practically capable catalysts for direct decomposition of high-concentration N_2O. The properties, including particle size, surface area, crystalline structure, reducibility, surface morphology, chemisorption, etc., were studied carefully to probe into the roles of TiO_2.

2. Experimental

2.1. Catalyst preparation

TiO_2 modified Al_2O_3 was prepared via excess-solution impregnation followed by spontaneous dispersion upon calcination. A calculated $Al(NO_3)_3{\cdot}6H_2O$ (Tianjin Chemical Reagent Co., Inc.) was dissolved in deionized water (typically 5 ml water and 5 ml ethanol per gram of TiO_2), and TiO_2 (P25, Degussa) was subsequently added. The slurry was further dispersed in an ultrasonic bath. After dried at 80 °C, the sample was collected and ground into fine powders, and then further calcined at a high temperature of 900 °C for 3 h (if not specially signified). The product was denoted as xTiO$_2$–Al_2O_3 (x = 0.2, 0.8, 1, 2 and 4), where x indicated the intended mol ratio of TiO_2 to Al_2O_3. Pure Al_2O_3 and TiO_2 were also obtained through calcination of dried solution of aluminum nitrate and TiO_2 (typically 5 ml water per gram of $Al(NO_3)_3{\cdot}6H_2O$) as referenced supports.

The above obtained supports were further impregnated with an aqueous solution of $H_2IrCl_6{\cdot}6H_2O$ to get the desired Ir loading of 5 wt%. The obtained samples were dried at 80 °C overnight and then calcined at 500 °C for 2 h in a muffle furnace in air atmosphere, designated as Ir/Al_2O_3, Ir/TiO_2 and Ir/xTiO$_2$–Al_2O_3.

To investigate the thermal stability of the catalysts, catalysts were again prepared with the same procedure as above, except that the iridium supported samples were calcined at high temperature of 1200 °C. The resultant catalysts were marked as Ir/Al_2O_3(HT), Ir/TiO_2(HT) and Ir/TiO_2–Al_2O_3(HT).

2.2. Catalyst characterization

BET surface areas of the catalysts were measured by N_2 adsorption at −196 °C using a Micromeritics ASAP 2010 apparatus. The X-ray diffraction (XRD) patterns were recorded with a PANalytical X'Pert-Pro powder X-ray diffractometer, using Cu Kα1 monochromatized radiation (λ = 0.1541 nm) at a scan speed of 5°/min.

Scanning electron microscopy (SEM) experiments were performed with a JSM 6360-LV electron microscope operating at 20 kV. The size of iridium particles was determined by transmission electron microscopy (TEM). A JEOL 2000 EX instrument was used, with an accelerating voltage of 120 kV. The samples were pretreated by reduction with pure H_2 for 0.5 h followed by passivation in a 5 vol% N_2O/Ar mixture. 200 particles were counted to calculate the size distribution.

Temperature-programmed reduction of H_2 (H_2-TPR) was performed on a Micromeritics Autochem 2920 apparatus. 35 mg of a sample was loaded into a U-shape quartz reactor and pretreated in a flow of Ar at 200 °C for 1 h. After cooling to 50 °C in Ar, the feed gas was switched to 10 vol% H_2–Ar mixture. Then, the sample was heated to 600 °C at a ramping rate of 10 °C min^{-1}. A thermal conductivity detector (TCD) was used on-line for measuring H_2 consumption. Ir dispersion was determined by H_2 pulse chemisorption uptake at room temperature. Before each experiment, the samples were reduced with H_2 at 400 °C for 0.5 h.

Oxygen adsorption was carried out with a BT2.15 heat-flux calorimeter as described elsewhere [38]. Prior to the measurement, the sample was heated to 400 °C in high pure H_2 (99.999%) atmosphere and held at that temperature for 0.5 h. After that, the sample was outgassed in a special treatment quartz cell at that temperature for 0.5 h under high vacuum. After being cooled to room temperature, the sample was transferred to a side-armed Pyrex vessel and sealed in a Pyrex capsule. The capsule can minimize the possible contamination in the high vacuum system in the course of thermal equilibrium (6–8 h) with the calorimeter. After thermal equilibrium was reached, the capsule was broken by a vacuum feedthrough and fresh catalyst was exposed. The microcalorimetric data were then collected by sequentially introducing small doses (1–10 μmol) of O_2 onto the sample until it became saturated (6–8 Torr).

2.3. Catalytic performance test

Activity evaluation was carried out in a fixed-bed flow quartz reactor with an inner diameter 6 mm as described in the literature [39]. Prior to the reaction, 100 mg (20–40 mesh) of a catalyst was reduced in H_2 at 400 °C for 0.5 h. After cooling to room temperature in Ar, the gas flow was switched to the reaction gas containing 30 vol% N_2O in Ar, and then passed through the catalyst at a flow rate of 50 ml/min (STP), corresponding to a gas hour space velocity (GHSV) of 30, 000 ml h^{-1} g_{cat}^{-1}. The reaction temperature was measured using a thermocouple located at the inlet of the catalyst bed. In view of exothermic effect of N_2O decomposition, each reaction temperature point was held for 0.5 h to ensure both the reaction and thermal environment reaching a steady state. The effluent gas was on-line analyzed by Agilent 6890N gas chromatograph equipped with a Porapak Q column and a Molecular Sieve 13X column. N_2O conversion was calculated based on the difference between its inlet and outlet concentrations.

3. Results and discussion

3.1. Effect of the support on N_2O decomposition

Fig. 1 shows the conversion of N_2O as a function of temperature in the presence of the catalyst Ir/Al_2O_3, Ir/TiO_2 and Ir/xTiO$_2$–Al_2O_3 (x = 0.2, 0.8, 1, 2 and 4). The samples, Ir/Al_2O_3 and Ir/TiO_2, exhibited reasonable activities compared to what have ever been evaluated under the same reaction conditions [18,39–41]. N_2O decomposition started at 300 °C and achieved 100% N_2O conversion at 450 °C. As for the catalysts with TiO_2 introduced, the catalytic activities were significant improved. Small amount of TiO_2 had an obvious promotive effect on N_2O decomposition. The catalytic activity was increased with increasing the titania content in the range of x = 0.2–1 and then decreased slowly at the higher content of TiO_2. In particular,

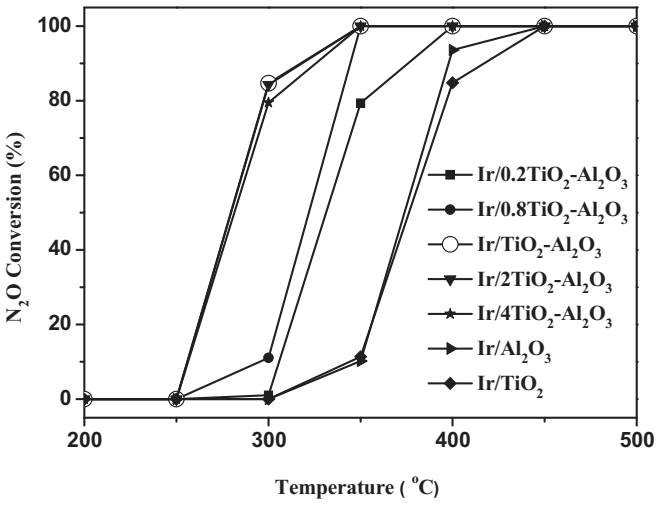

Fig. 1. N_2O conversion as a function of temperature over Ir/xTiO$_2$–Al$_2$O$_3$, Ir/TiO$_2$ and Ir/Al$_2$O$_3$ catalysts.

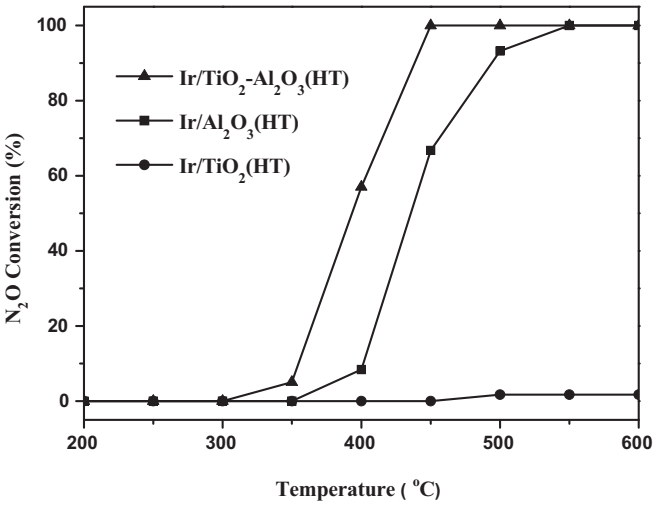

Fig. 3. N_2O conversions as a function of temperature over the Ir catalysts calcined at 1200 °C.

the Ir/TiO$_2$–Al$_2$O$_3$ (when x = 1, not shown hereinafter) exhibited a very high activity in N_2O decomposition, initiating the decomposition at 250 °C and achieving 100% conversion at 350 °C, very close to the highest activity that have ever been reported by Zhao et al. [18]. According to the above, the xTiO$_2$–Al$_2$O$_3$ composite was assumed to be a more suitable support for Ir catalysts used for N_2O decomposition.

The effect of calcination temperature of the support on N_2O conversion was subsequently investigated over the Ir/TiO$_2$–Al$_2$O$_3$ catalyst. The results are shown in Fig. 2. It could be found that with the increase of the calcination temperature of the support, N_2O conversion decreased slowly. Even so, the Ir/TiO$_2$–Al$_2$O$_3$ catalysts demonstrated higher activities than those of the Ir/Al$_2$O$_3$ and Ir/TiO$_2$ catalysts given in Fig. 1.

Thermal stability was investigated as well by evaluating the catalytic activities of the catalysts calcined at high temperature of 1200 °C. As illustrated in Fig. 3, a significant decrease in N_2O decomposition reactivity was observed. Among the selected catalysts, the Ir/TiO$_2$–Al$_2$O$_3$(HT) exhibited the highest activity for N_2O decomposition, revealing its fairly good thermal stability after high-temperature calcination. The Ir/Al$_2$O$_3$(HT) gave a relatively lower activity, and the Ir/TiO$_2$(HT) was almost inactive under the described reaction condition.

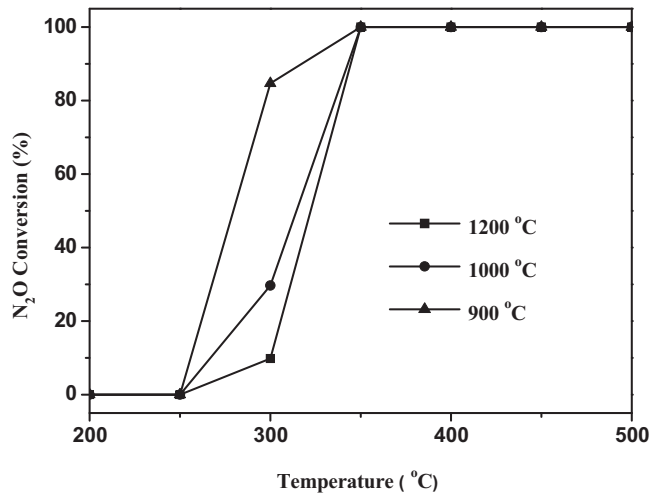

Fig. 2. N_2O conversions as a function of temperature over the Ir catalysts with the support calcined at different high temperatures.

In order to understand the role of TiO$_2$ in the Ir/TiO$_2$–Al$_2$O$_3$ catalyst, structure and surface characteristics were compared among the Ir/TiO$_2$–Al$_2$O$_3$, Ir/Al$_2$O$_3$ and Ir/TiO$_2$ catalysts using the techniques of XRD, BET, H_2 pulse chemisorption, TEM, SEM, TPR, and O_2 adsorption microcalorimetry.

3.2. Physical properties of the catalysts

The XRD patterns of the Ir/TiO$_2$–Al$_2$O$_3$, Ir/Al$_2$O$_3$ and Ir/TiO$_2$ catalysts are presented in Fig. 4. The peaks of Ir/TiO$_2$ showed a typical rutile phase of TiO$_2$ (JCPDS: 01-089-4202), and those of Ir/Al$_2$O$_3$ were mainly assigned to the γ-Al$_2$O$_3$ phase (JCPDS: 00-010-0425). IrO$_2$ phase (JCPDS: 01-088-0288) was also detected in both samples with the average size of 14 nm and 13 nm, calculated from the most intense IrO$_2$ line at 2θ = 34.5° using Scherrer's formula (Table 1). The XRD pattern of Ir/TiO$_2$–Al$_2$O$_3$ showed a mixed structure, where TiO$_2$ is in rutile form and Al$_2$O$_3$ in α-Al$_2$O$_3$ phase. No diffraction lines due to iridium species were identified. The XRD result of Ir/TiO$_2$–Al$_2$O$_3$ inferred that the phase transition to α-Al$_2$O$_3$ phase of alumina was promoted by the addition of TiO$_2$ and iridium was highly dispersed on the binary oxide support. It was really sur-

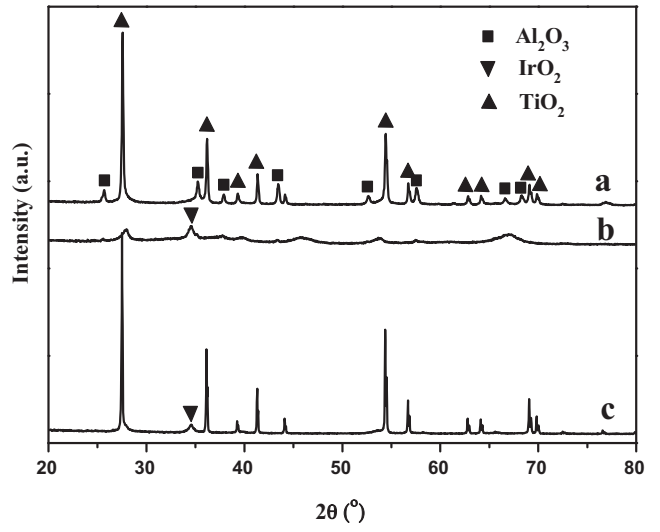

Fig. 4. X-ray diffraction patterns of the catalyst: Ir/TiO$_2$–Al$_2$O$_3$ (a), Ir/Al$_2$O$_3$ (b), and Ir/TiO$_2$ (c).

Table 1
Properties of the $Ir/TiO_2–Al_2O_3$, Ir/Al_2O_3, and Ir/TiO_2 catalysts.

Properties	$Ir/TiO_2–Al_2O_3$	Ir/Al_2O_3	Ir/TiO_2
BET (m^2/g)	17	74	4
Ir dispersion (%)	33	19	8

prising because α-Al_2O_3 was seldom formed under the calcination of 900 °C and iridium should aggregate on α-Al_2O_3 and present the diffraction peaks, owing to the small surface area and poor pore structure of α-Al_2O_3. More interestingly, the $Ir/TiO_2–Al_2O_3$ catalyst possessed the highest catalytic activity in this study in N_2O decomposition, contrary to the normal understanding that α-Al_2O_3 was avoided utilizing as a catalyst support. For this reason, a strong interest was inspired to further explore the physicochemical properties of the catalyst and the role of TiO_2.

BET surface areas of the $TiO_2–Al_2O_3$, Al_2O_3, and TiO_2 supported iridium samples are listed in Table 1. The surface area of Ir/Al_2O_3 was 74 m^2/g, and the value decreased to 17 m^2/g for $Ir/TiO_2–Al_2O_3$. Pure TiO_2 supported iridium was with the smallest surface area in these catalysts. It was noted that the introduction of TiO_2 caused a great decrease in the surface area, similar to that reported in the literatures [35,37,42]. Thus, the factor of BET surface area appeared not responsible for the enhancement of the catalytic activity.

Ir dispersions were also examined with the ordinary H_2 pulse chemisorption method (Table 1). The $Ir/TiO_2–Al_2O_3$ catalyst showed the highest Ir dispersion (33%) among the catalysts presented here, whereas the Al_2O_3 and TiO_2 based catalysts showed very low Ir dispersions. The results of Ir dispersions matched very well with the catalytic activities of the catalysts for N_2O decomposition.

3.3. TEM and SEM morphologies

TEM images of the $Ir/TiO_2–Al_2O_3$, Ir/Al_2O_3 and Ir/TiO_2 catalysts were shown in Fig. 5. Agglomerated iridium particles with the diameter of about 10 nm were observed in the pure Al_2O_3 or TiO_2 based catalysts, quite in agreement with those obtained by Scherrer's formula. Iridium nanoparticles were uniformly and highly dispersed on the $Ir/TiO_2–Al_2O_3$ catalyst, with a mean particle size of 2.3 nm as depicted in the particle size distribution in Fig. 6. Obviously, these results coincided with that obtained from XRD and H_2 pulse chemisorption measurements. The drastic decrease of Ir particle size was believed to be closely correlated with the distinct activity enhancement on the $Ir/TiO_2–Al_2O_3$ catalyst.

Generally speaking, the metal dispersion varied in line with the total surface area of the sample, while in this research, the binary oxide supported catalyst had a small iridium size and high Ir dispersion with a low surface area, in comparison to the simplex Al_2O_3 and TiO_2. Accordingly, it could be deduced that the support played a decisive part in stabilizing of the iridium species as well as improving the catalytic activity. In order to further investigate the surface property of the support, SEM measurement was conducted on Al_2O_3, TiO_2 and $TiO_2–Al_2O_3$. It can be seen from the micrographs in Fig. 7 that the binary oxide support presented nanoscale roughness structure on the surface of the sample grain, whereas the simplex Al_2O_3 and TiO_2 demonstrated almost smooth and clean surfaces. Meanwhile, single TiO_2 particle was comparatively small, and therefore formed a large number of edges and irregular shapes on the bulk support. A careful observation of the binary oxide revealed that the external surface of the sample was full of irregular aggregates. Similar small aggregates had also been observed on the mixed oxides as described by Vargas et al. [43]. The main roles of the nanoscale irregular aggregates are thought to be twofold. On the one hand, the nanoscale irregular aggregates could behave as a migration barrier on the oxide substrate.

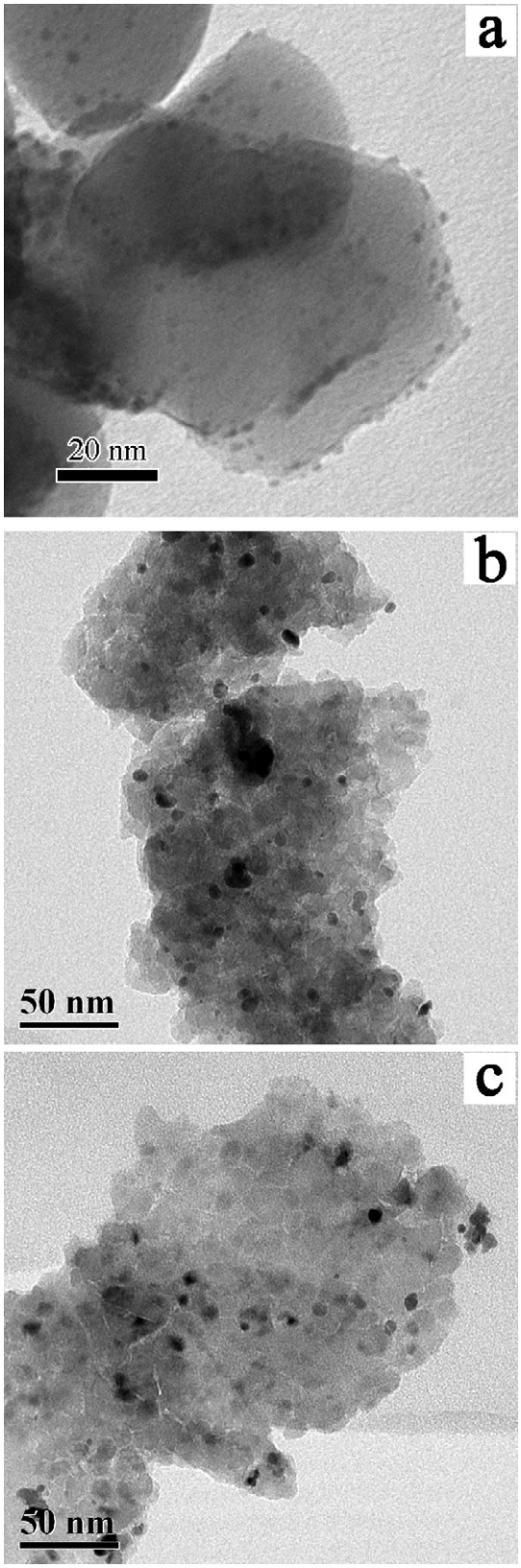

Fig. 5. Morphologies of the Ir particles in the catalyst: $Ir/TiO_2–Al_2O_3$ (a), Ir/Al_2O_3 (b), and Ir/TiO_2 (c).

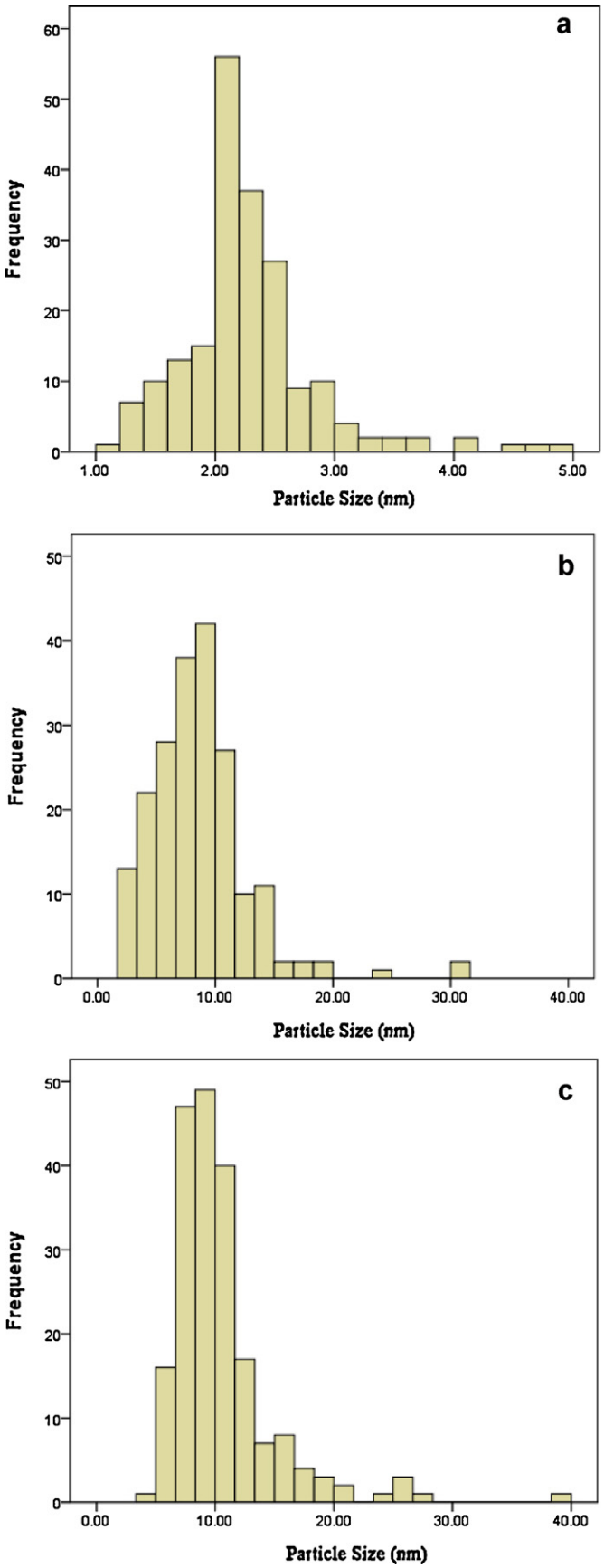

Fig. 6. Size distributions of Ir particles: Ir/TiO_2–Al_2O_3 (a), Ir/Al_2O_3 (b), and Ir/TiO_2 (c).

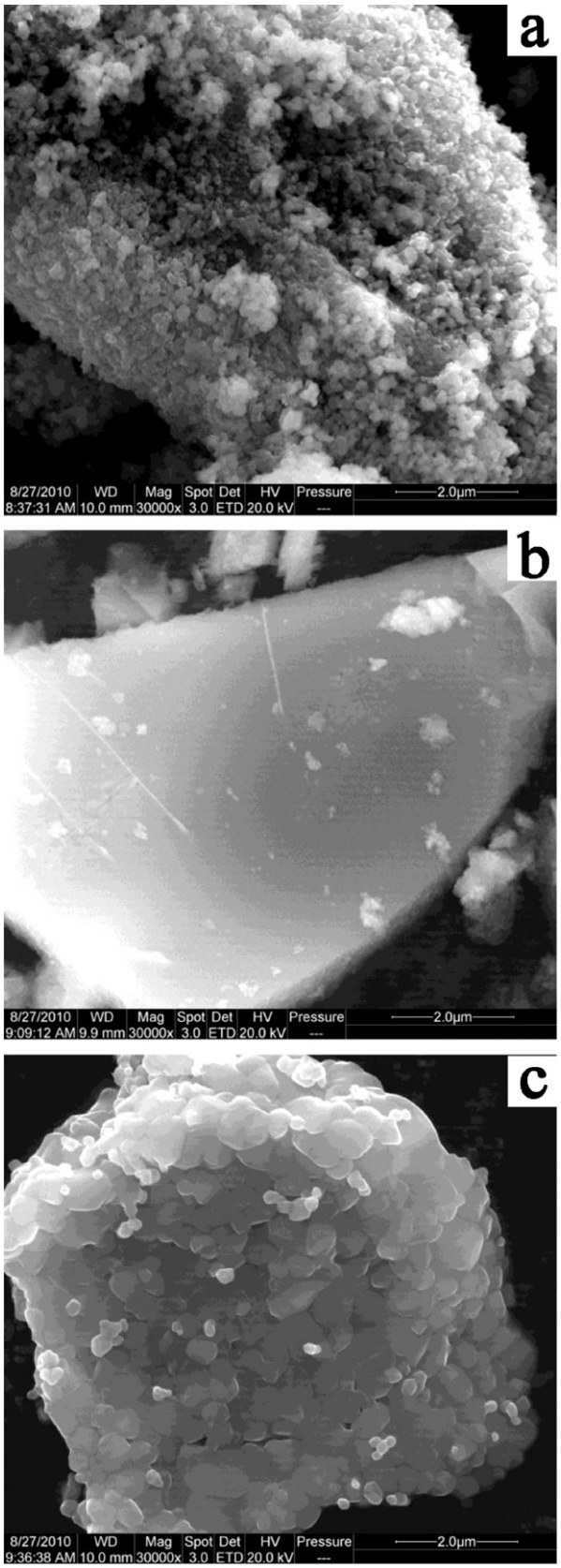

Fig. 7. SEM micrographs of the support: TiO_2–Al_2O_3 (a), Al_2O_3 (b), and TiO_2 (c).

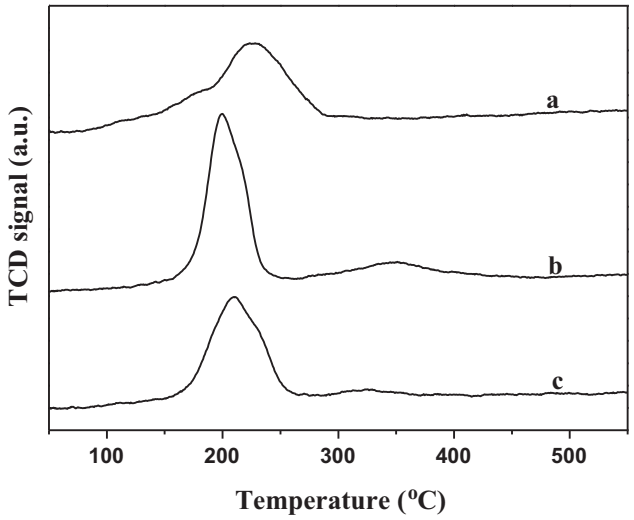

Fig. 8. TPR profiles of the catalyst: $Ir/TiO_2–Al_2O_3$ (a), Ir/Al_2O_3 (b), and Ir/TiO_2 (c).

The barrier decorated the perimeter sites of the active phase, and thereby prevented the migration of Ir atom on the surface during calcination and/or reaction process and inhibited Ir nanoparticle growth and/or sintering. Rashkeev et al. [44] have found similar blocking effect of the atomic-scale roughness on the Au/TiO_2 catalysts, which retarded the atomic surface diffusion and inhibited Au nanoparticle growth and/or sintering by introducing an additional atomic thick SiO_2 layer, investigated via comprehensive theoretical/computational study. On the other hand, the nanoscale irregular aggregates could result in a great anchoring strength of the active phase. Extra interaction between the impregnated Ir species and the support was thus formed to better retain the active phase. In a word, the nanoscale irregular aggregates of the binary oxide support could well explain the small size or high dispersion of iridium and the high catalytic activity of the $Ir/TiO_2–Al_2O_3$ catalyst for N_2O decomposition.

3.4. Reduction ability of the catalysts

Fig. 8 illustrates the TPR profiles of the $Ir/TiO_2–Al_2O_3$, Ir/Al_2O_3 and Ir/TiO_2 catalysts. It can be noticed that the reduction temperature changed with the supports. The $Ir/TiO_2–Al_2O_3$ catalyst presented a broad reduction peak of the hydrogen consumption centered at 229 °C. In contrast, the reduction peaks of the Ir/Al_2O_3 and Ir/TiO_2 catalysts were shifted to lower temperatures. The presence of TiO_2 in the $Ir/TiO_2–Al_2O_3$ catalyst deferred the reduction of iridium oxide. This indicated that a strong interaction between Ir species and the support existed; confirming the suggestion that iridium particles were decorated with the irregular aggregates of the support deduced from the SEM images.

3.5. Microcalorimetry of O_2 adsorption

In order to obtain a further understanding of the promotive effect of TiO_2 on Ir/Al_2O_3 catalyst for N_2O decomposition, microcalorimetry technique was applied to quantitatively measure the chemisorption properties of the Ir based catalysts. Taking into account that O_2 is a product of N_2O decomposition and its desorption was regarded as the rate determining step [45], O_2 was chosen as the probe molecule to compare the different adsorption heat and adsorption amount among the $Ir/TiO_2–Al_2O_3$, Ir/Al_2O_3 and Ir/TiO_2 catalysts.

Fig. 9 displays the results of microcalorimetric measurements. O_2 adsorption on Ir/Al_2O_3 at room temperature produced an initial

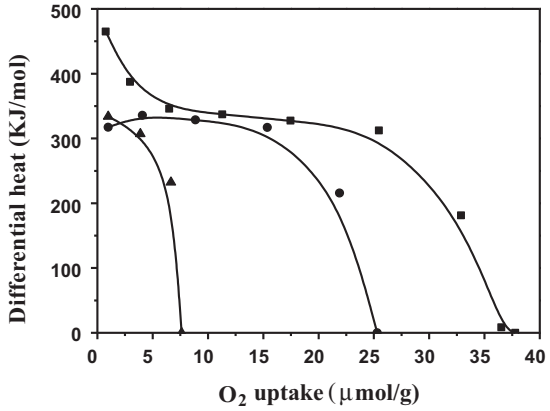

Fig. 9. Differential heats of O_2 adsorption versus O_2 uptake on $Ir/TiO_2–Al_2O_3$ (■), Ir/Al_2O_3 (●), and Ir/TiO_2 (▲) catalysts.

heat of 318 kJ/mol, which was consistent with the value reported on other Ir/Al_2O_3 catalysts [46]. The differential heat versus O_2 uptake remained almost constant at 320 kJ/mol up to 15 μmol/g and then decreased to the saturation uptake of ca. 25 μmol/g. Similar differential heat was obtained on Ir/TiO_2, but the O_2 uptake was quite low, only 7 μmol/g in saturation uptake of O_2 adsorption. Unlike Ir/Al_2O_3 and Ir/TiO_2, the Ir/Al_2O_3-TiO_2 catalyst demonstrated an obviously high initial heat, and the saturation uptake of O_2 was also greatly increased. Obviously, the $Ir/TiO_2–Al_2O_3$ catalyst possessed different iridium species and a larger number of oxygen coverage sites than Ir/Al_2O_3 and Ir/TiO_2.

Further microcalorimetry experiments were performed on the samples pretreated with N_2O and then adsorbed with O_2. With such a treatment, strong adsorption sites could be occupied by the dissociative oxygen generated from N_2O. As a consequence, this adsorption of oxygen could be regarded as the reversible adsorption of oxygen, which could reflect the recombination and desorption ability of the oxygen during the N_2O decomposition process. As seen from Fig. 10, the adsorption heat and saturation uptake of O_2 adsorption all decreased greatly. Strikingly, the $Ir/TiO_2–Al_2O_3$ catalyst remained the highest amount of the saturation uptakes of O_2 compared to those of the other two samples, indicating the best capability of O_2 adsorption among the three catalysts. We have described previously that N_2O decomposes via a redox mechanism, with oxygen desorption from the catalyst surface as the rate determining step. Hence, the favouring of reversible oxygen adsorption

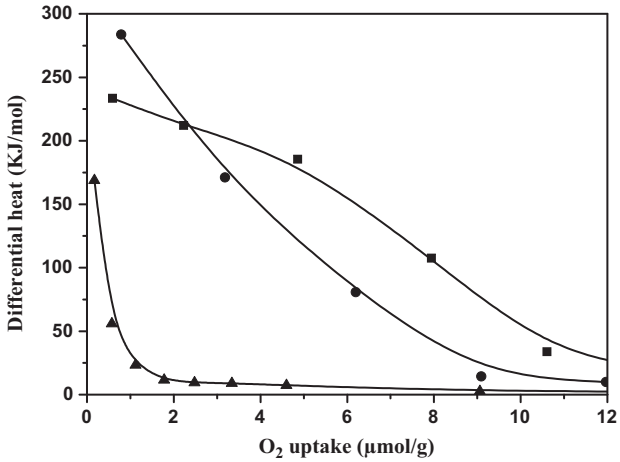

Fig. 10. Differential heats of O_2 adsorption after preadsorbing N_2O versus O_2 uptake on the catalysts of $Ir/TiO_2–Al_2O_3$ (■), Ir/Al_2O_3 (●), and Ir/TiO_2 (▲).

on the TiO_2–Al_2O_3 sample can be ascribed to another main reason of the superior catalytic activity of the catalyst.

4. Conclusions

The TiO_2 promoted Ir/Al_2O_3 catalyst was prepared and exhibited a high catalytic activity and a good thermal stability in N_2O decomposition. Uniform and highly dispersed Ir particles were detected on the Ir/TiO_2–Al_2O_3 catalyst and directly accountable for the activity enhancement in N_2O decomposition. Nanoscale irregular aggregates induced by TiO_2 addition were assumed to act as obstacles to migration of iridium and protectors against sintering. A strong interaction between iridium and the support was also revealed because of the unique structure of the TiO_2 promoted Ir/Al_2O_3 catalyst. In addition, the introduction of TiO_2 led to a distinct change in chemisorption properties. The favouring of oxygen adsorption can be regarded as another main reason for the superior catalytic activity of the TiO_2 promoted sample.

Acknowledgements

Supports of National Science Foundation of China (No. 20973165, No. 20773122) and External Cooperation Program of Chinese Academy of Sciences (GJHZ200827) are gratefully acknowledged.

References

[1] K. Asano, C. Ohnishi, S. Iwamoto, Y. Shioya, M. Inoue, Appl. Catal. B: Environ. 78 (2008) 242–249.
[2] H.Q. Jiang, H.H. Wang, F.Y. Liang, S. Werth, T. Schiestel, J. Caro, Angew. Chem. Int. Ed. 48 (2009) 2983–2986.
[3] J. Perez-Ramirez, M. Santiago, Chem. Commun. (2007) 619–621.
[4] J. Perez-Ramirez, E.V. Kondratenko, Chem. Commun. (2004) 376–377.
[5] V. Zakirov, L. Li, Tsinghua Sci. Technol. 11 (2006) 507–514.
[6] V. Zakirov, M. Sweeting, T. Lawrence, J. Sellers, Acta Astronaut. 48 (2001) 353–362.
[7] V. Zakirov, H. Zhang, J. Aerosp. Eng. 222 (2008) 103–108.
[8] V. Zakirov, H.Y. Zhang, Aerosp. Sci. Technol. 12 (2008) 318–323.
[9] F.J. Perez-Alonso, I. Melian-Cabrera, M.L. Granados, F. Kapteijn, J.L.G. Fierro, J. Catal. 239 (2006) 340–346.
[10] A. Scagnelli, C. Di Valentin, G. Pacchioni, Surf. Sci. 600 (2006) 386–394.
[11] L. Xue, C.B. Zhang, H. He, Y. Teraoka, Appl. Catal. B: Environ. 75 (2007) 167–174.
[12] G. Centi, P. Generali, L. dall'Olio, S. Perathoner, Z. Rak, Ind. Eng. Chem. Res. 39 (2000) 131–137.
[13] N. Labhsetwar, M. Dhakad, R. Biniwale, T. Mitsuhashi, H. Haneda, P.S.S. Reddy, S. Bakardjieva, J. Subrt, S. Kumar, V. Kumar, P. Saiprasad, S. Rayalu, Catal. Today 141 (2009) 205–210.
[14] K. Sun, H. Xia, E. Hensen, R. van Santen, C. Li, J. Catal. 238 (2006) 186–195.
[15] J.P. Dacquin, C. Dujardin, P. Granger, Catal. Today 137 (2008) 390–396.
[16] C. Ohnishi, S. Iwamoto, M. Inoue, Chem. Eng. Sci. 63 (2008) 5076–5082.
[17] S. Parres-Esclapez, M.J. Illan-Gomez, C.S.M. de Lecea, A. Bueno-Lopez, Appl. Catal. B: Environ. 96 (2010) 370–378.
[18] X.Y. Zhao, Y. Cong, F. Lv, L. Li, X.D. Wang, T. Zhang, Chem. Commun. 46 (2010) 3028–3030.
[19] J.R. Wallbank, P.A. Sermon, A.M. Baker, L. Courtney, R.M. Sambrook, The 2nd International Conference on Green Propellants for Space Propulsion, 2004, p. 7.
[20] S. Mary, C. Kappenstein, S. Balcon, S. Rossignol, E. Gengembre, Appl. Catal. A: Gen. 182 (1999) 317–325.
[21] A. Barrera, J.A. Montoya, M. Viniegra, J. Navarrete, G. Espinosa, A. Vargas, P. del Angel, G. Perez, Appl. Catal. A: Gen. 290 (2005) 97–109.
[22] A. Barrera, M. Viniegra, S. Fuentes, G. Diaz, Appl. Catal. B: Environ. 56 (2005) 279–288.
[23] S. Fuentes, N. Bogdanchikova, M. Avalos-Borja, A. Boronin, M.H. Farias, G. Diaz, A.G. Cortes, A. Barrera, Catal. Today 55 (2000) 301–309.
[24] L. Courtheoux, D. Amariei, S. Rossignol, C. Kappenstein, Appl. Catal. B: Environ. 62 (2006) 217–225.
[25] L. Courtheoux, E. Gautron, S. Rossignol, C. Kappenstein, J. Catal. 232 (2005) 10–18.
[26] A.F. Popa, S. Rossignol, C. Kappenstein, J. Mater. Chem. 12 (2002) 2866–2868.
[27] S. Colussi, F. Arosio, T. Montanari, G. Busca, G. Groppi, A. Trovarelli, Catal. Today 155 (2010) 59–65.
[28] J. Haber, T. Machej, J. Janas, M. Nattich, Catal. Today 90 (2004) 15–19.
[29] J. Haber, M. Nattich, T. Machej, Appl. Catal. B: Environ. 77 (2008) 278–283.
[30] B.M. Reddy, B. Chowdhury, P.G. Smirniotis, Appl. Catal. A: Gen. 211 (2001) 19–30.
[31] J. Jia, J. Zhou, C. Zhang, Z. Yuan, S. Wang, L. Cao, S. Wang, Appl. Catal. A: Gen. 341 (2008) 1–7.
[32] W.Q. Xu, H. He, Y.B. Yu, J. Phys. Chem. C 113 (2009) 4426–4432.
[33] W.F. Yan, S.M. Mahurin, Z.W. Pan, S.H. Overbury, S. Dai, J. Am. Chem. Soc. 127 (2005) 10480–10481.
[34] W. Lin, Y.X. Zhu, N.Z. Wu, Y.C. Xie, I. Murwani, E. Kemnitz, Appl. Catal. B: Environ. 50 (2004) 59–66.
[35] A.J. Duan, R.L. Li, G.Y. Jiang, J.S. Gao, Z. Zhao, G.F. Wan, D.Q. Zhang, W.Q. Huang, K.H. Chung, Catal. Today 140 (2009) 187–191.
[36] J.H. Li, Y.Q. Zhu, R. Ke, J.M. Hao, Appl. Catal. B: Environ. 80 (2008) 202–213.
[37] N. Macleod, R. Cropley, J.M. Keel, R.M. Lambert, J. Catal. 221 (2004) 20–31.
[38] H.K. Cheng, Y.Q. Huang, A.Q. Wang, L. Li, X.D. Wang, T. Zhang, Appl. Catal. B: Environ. 89 (2009) 391–397.
[39] S.M. Zhu, X.D. Wang, A.Q. Wang, T. Zhang, Catal. Today 131 (2008) 339–346.
[40] M. Tian, A.Q. Wang, X.D. Wang, Y.Y. Zhu, T. Zhang, Appl. Catal. B: Environ. 92 (2009) 437–444.
[41] S.M. Zhu, X.D. Wang, A.Q. Wang, Y. Cong, T. Zhang, Chem. Commun. (2007) 1695–1697.
[42] B.M. Reddy, K.N. Rao, G.K. Reddy, P. Bharah, J. Mol. Catal. A: Chem. 253 (2006) 44–51.
[43] A. Vargas, J.A. Montoya, C. Maldonado, I. Hernandez-Perez, D.R. Acosta, J. Morales, Micropor. Mesopor. Mater. 74 (2004) 1–10.
[44] S.N. Rashkeev, S. Dai, S.H. Overbury, J. Phys. Chem. C 114 (2010) 2996–3002.
[45] S. Alini, F. Basile, S. Blasioli, C. Rinaldi, A. Vaccari, Appl. Catal. B: Environ. 70 (2007) 323–329.
[46] L. Li, X.D. Wang, X.Q. Zhao, M.Y. Zheng, R.H. Cheng, L.X. Zhou, T. Zhang, Thermochim. Acta 434 (2005) 119–124.